AMERICAN JOURNAL OF
MATERIALS AND
NANOTECHNOLOGY

Zr^{4+}-Doped Anatase TiO_2 Nanotube Array Electrode for Electrocatalytic Reduction of L-cystine

Weizhen Wang, Guangxin Wang, Xuhui Zhao *, Xiaofeng Zhang, Yuming Tang * and Yu Zuo

Beijing Key Laboratory of Electrochemical Process and Technology for Materials, Beijing University of Chemical Technology, Beijing 100029, China

Abstract: A Zr^{4+}-doped anatase TiO_2 nanotube array electrode was prepared using a process that included Ti anodizing, chemical immersion, and heat treatment. The compositions, microstructure, and electrochemical properties of the prepared electrodes were characterized. The results show that Zr^{4+} was successfully introduced into the TiO_2 nanotube array electrodes. Because Zr^{4+} was doped into the crystal structure of the $TiO_2$and replaced a part of Ti^{4+} to form more oxygen vacancies and Ti^{3+}, the electrocatalytic activity of the prepared electrodes, for the reduction of L-cystine, was significantly improved.

Keywords: nanocomposites; oxidation; titanium dioxide; electrocatalysis

---

1. Introduction

L-cysteine is widely used in many fields, such as medicine, cosmetics, and biochemical research. The typical industrial production of L-cysteine is achieved through the electrocatalytic reduction of L-cystine. The currently used Pb electrodes, or other catalytic electrodes with deposited Pb, are prone to heavy metal pollution in acid electrolytes. Although titanium electrodes have also been used in the reduction of L-cystine, the effect is not satisfactory [1]. Therefore, developing alternative materials with stable performance, that are environmentally friendly and have a high catalytic reduction activity, are one of the current research hotspots [2–4].

As one of the most studied catalytic materials, TiO_2 has an important role in the field of catalysis [5–11]. Skúlason et al. [12] discussed the role of transition metal oxides in the electrocatalytic reduction of N_2 by using density functional theory (DFT) calculations. Hirakawa et al. [13] reported the role of oxygen vacancies and Ti^{3+} in TiO_2 in the photocatalytic reduction of N_2. In order to enhance the catalytic activity of TiO_2, doping metal elements are used to increase the vacancies and defects in the TiO_2 crystal structure [14–17]. At present, most of the correlative research in this field mainly focuses on the photocatalysis of TiO_2. However, there are relatively few studies on its electrocatalysis, especially regarding electrocatalytic reduction. Recently, Cao et al. [18,19] reported in detail that a Zr^{4+}-doped TiO_2 electrode can efficiently reduce N_2 through electrocatalysis. This provides a feasible idea from which we can design a TiO_2 nanotube array electrode with a high electrocatalytic reduction activity for reducing L-cystine. Moreover, considering the better stability of titanium and the existence of the oxygen vacancies and Ti^{3+} in the anatase TiO_2, the TiO_2 nanotube array electrode might also possess good potential in the field of electrocatalytic reduction.

We have designed a Zr^{4+}-doped anatase TiO_2 nanotube array electrode (anatase Zr/TiO_2), in which Zr^{4+} partly replaces Ti^{4+} in the anatase TiO_2, and studied its electrocatalytic reduction activity for reducing L-cystine and discussed its reduction mechanism.

2. Materials and Methods

The preparation process for the anatase Zr/TiO2 electrode is shown in Figure 1a. Firstly, the TiO2 nanotube arrays on the pure Ti foil (99.99 wt%) surface was prepared through anodizing, which was carried out in 35 wt% (CH2OH)2 (ethylene glycol) + 0.5 wt% HF (hydrofluoric acid) solutions, under, under constant voltage of 20 V for 35 min at room temperature. The auxiliary electrode was a graphite a constant voltage of 20 V for 35 min at room temperature. The auxiliary electrode was a graphite electrode. After anodization, the samples were soaked in deionized water and then chemically electrode. After anodization, the immersed in a 0.3 mol L 1 Zr(NO3)4 solution for 4 h, in order to dope Zr4+ . Subsequently, the samples immersed in a 0.3 mol·L−1 Zr(NO3)4 solution for 4 h, in order to dope Zr4+. Subsequently, the samples were washed with deionized water and ethanol, several times. Finally, they were heated to 450 C, were washed with deionized water and ethanol, several times. Finally, kept for two hours, and cooled slowly in a muffle furnace.

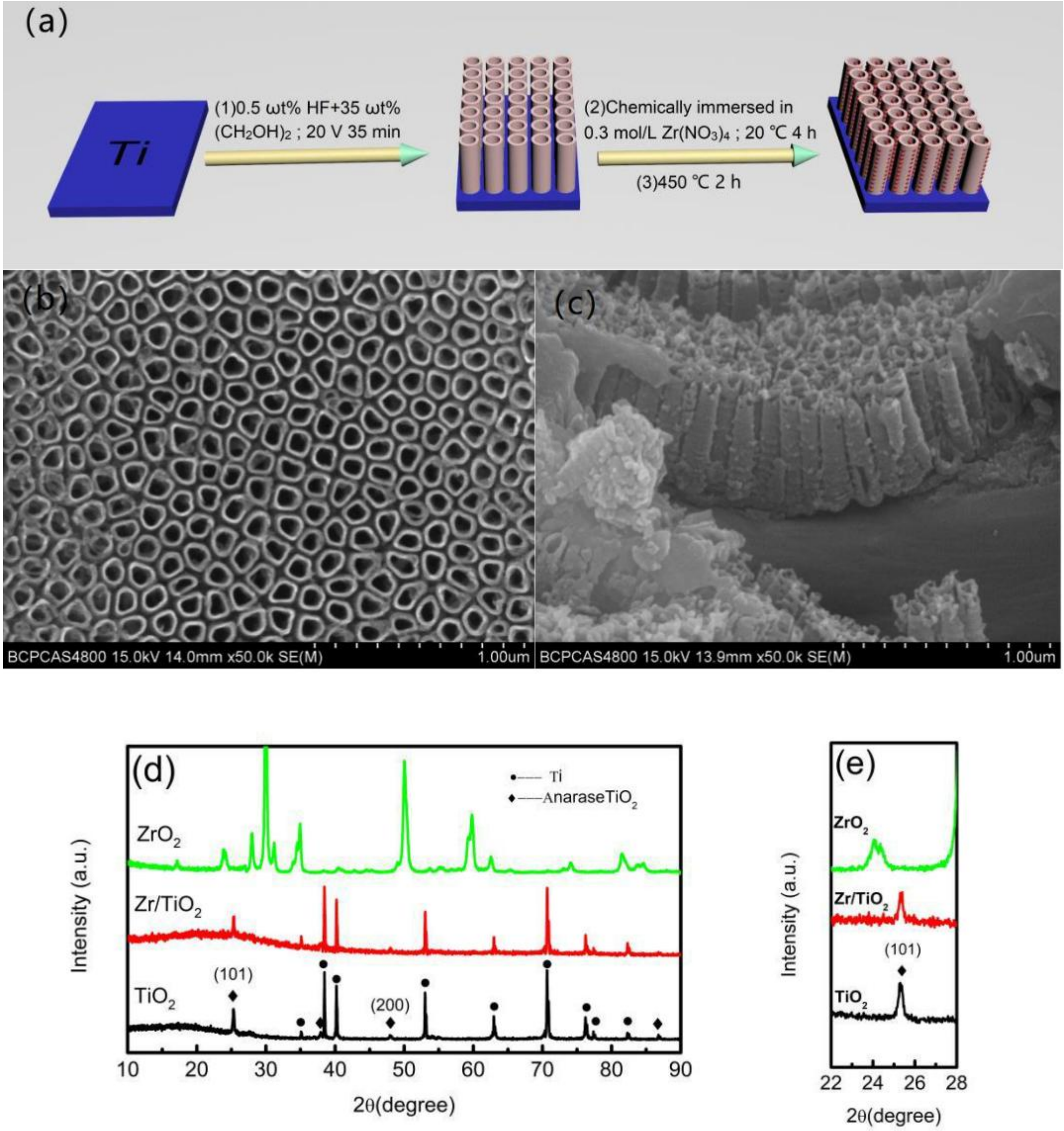

Figure 1. Preparation process (**a**), surface (**b**), and section (**c**) morphologies, and XRD patterns (**d**,**e**) of anatase Zr/TiO_2 nanotube array electrode. anatase Zr/TiO2 nanotube array electrode.

The crystal structure of the modified electrode surface was studied using X- ray diffraction (XRD) (Bruker D8 advance, Cu K , = 0.1548 nm, Berlin, Germany). The morphology, length, and diameter (Bruker D8 advance, Cu Kα, λ = 0.1548 nm, Berlin, Germany). The morphology, length, and diameter of the TiO_2 nanotubes on the electrode surface were characterized using a SEM (S-4800, Hitachi, Tokyo, Japan). The existence and valence of Ti and Zr on the surface of the Zr/TiO_2 electrode were characterized using X-ray photoelectron spectroscopy (XPS) (PHI 1600 ESCA, PerkinElmer, Waltham, MA, USA). The binding energies of the peaks were calibrated using the binding energy of the C1s peak (285 eV).

The electrochemical performance was tested using the electrochemical workstation (CS350H, Wuhan Corrtest, Wuhan, China). In the three-electrode system, the auxiliary electrode was a Pt electrode, and the reference electrode was a saturated calomel electrode. The test solutions were HCl solutions containing L-cystine.

3. Results

Scanning electron microscopy (SEM) images show that the anatase Zr/TiO_2 electrode has a tubular structure, with tube diameters and lengths of about 100 and 650 nm, respectively (Figure 1b,c). The crystalline structures of the different samples were studied using X-ray diffraction (Figure 1d)—for both the undoped and Zr^{4+}-doped TiO_2 nanotube arrays. The other diffraction peaks correspond to the anatase phase (JCPDS # 21-1272). A close examination of the pattern (Figure 1e), after doping Zr^{4+}, revealed that the peak intensity of the TiO_2 slightly decreased. According to the Scherrer equation, the calculated grain sizes of the TiO_2 (101) were about 7 and 5.1 nm for the undoped and doped samples, respectively, suggesting that the grain sizes of the TiO_2 also became slightly smaller after doping Zr^{4+}. Above, the results indicate that the crystallinity of the TiO_2 slightly decreased. No diffraction peak relating to the ZrO_2 was observed in the XRD pattern (JCPDS # 79-1768). Compared to Ti^{4+}, Zr^{4+} is suitable in size, and is similar in d electron configuration and oxide structure (Zr^{4+} 72 pm, Ti^{4+} 52 pm) [15]. Zr^{4+} was doped into the anatase TiO_2 to replace a part of Ti^{4+}, and did not change the anatase crystal structure [18].

X-ray photoelectron spectroscopy (XPS) was used to characterize the chemical composition of the electrode surface. Figure 2 shows an overview of the XPS spectra for the undoped and Zr^{4+} doped TiO_2 nanotube array electrodes. The Zr^{4+} doped electrode surface is mainly composed of Ti and O, containing a small amount of Zr (about 2.44 atom. %). The peak of C1s may be attributed to the contaminants on the sample surface. In addition, the binding energies of the peaks were calibrated by the binding energy of the C1s peaks (285 eV). The Zr 3D spectra (Figure 3a) show two obvious peaks, revealing that the Zr element was on the surface of the electrode. However, there was no diffraction peak of ZrO_2 in the XRD pattern (Figure 1d), and the peak intensity of the TiO_2 slightly decreased; its peak positions moved slightly to the right after the doping of Zr4+ (Figure 1e), indicating that the Zr should be incorporated into the TiO_2 crystal lattice [20,21]. Figure 3b shows the deconvoluted XPS spectrum for the Ti 2p region. From the XPS-peak-differentiating analysis, it was found that, regardless of Zr^{4+}-doping or not, Ti^{3+} and Ti^{4+} exist in the TiO_2 electrodes. The four peaks correspond to the Ti^{3+} 2p3/2 (457.65 eV), Ti^{4+} 2p3/2 (458.95 eV), Ti^{3+} 2p1/2 (463.10 eV), and Ti^{4+} 2p1/2 (464.66 eV) [20]. However, for the undoped TiO_2 nanotube array electrode, the Ti^{3+} content is very small (about 4.9 atom% of the total Ti). For the Zr^{4+}-doped electrode, there is a significant increase in the area of two Ti^{3+} sub-peaks in Figure 3b, indicating an increase in the Ti^{3+} content (about 14.1 atom% of the total Ti). Compared with Figure 3c,d, the onset potential of the amorphous TiO_2 nanotube array electrode for a hydrogen evolution reaction (HER) is significantly more negative than that of the pure titanium electrode, but no other redox peak was observed in the cyclic voltammetries (CVs) for both electrodes. However, for the undoped and Zr^{4+}-doped anatase TiO_2 nanotube array electrodes, there were nearly reversible redox peaks in the CVs, which corresponded to a transformation between Ti^{4+} and Ti^{3+} [22]. Moreover, after doping Zr^{4+}, the oxidation peak current decreased, and reduction peak current increased, which indicated that it is beneficial to transform Ti^{4+} into Ti^{3+} on the anatase Zr/TiO_2 nanotube array electrode. This is consistent with the previous XPS results.

Figure 2. XPS spectra of TiO2 nanotube array surface: (**a**) Zr^{4+} doped; (**b**) undoped.

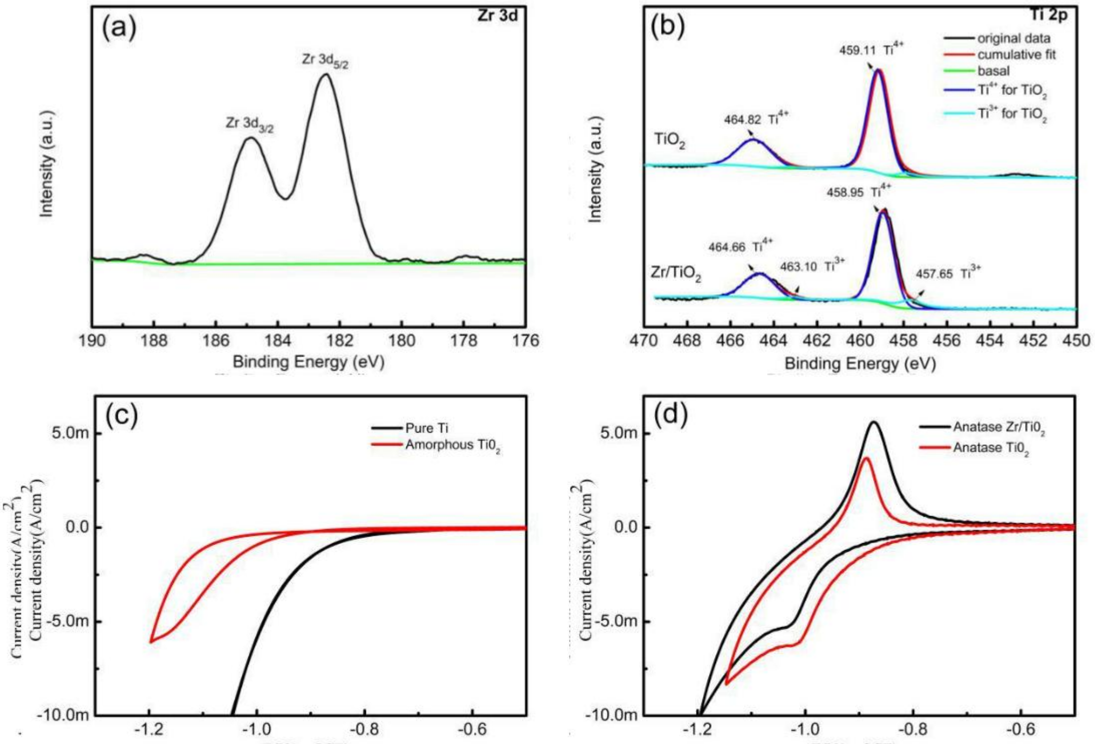

found during cathodic polarization, and the reduction current increased after doping Zr4+, as shown in Figure 4c,d. This indicates that the anatase structure of TiO2 is helpful in the formation of Ti3, and in Figure 4c,d. This indicates that the anatase structure of TiO2 is helpful in the formation of Ti3, and as shown in Figure 4c,d. This indicates that the anatase structure of TiO_2 is helpful in the formation of Ti^3, and the dopant of Zr^{4+} can accelerate the transformation of Ti^{4+} to Ti^{3+}. Moreover, when adding L-cystine to HCl solutions, the reduction currents increase in the two anatase TiO2 nanotube array electrodes, before hydrogen evolution is observed, which suggests that the anatase TiO possesses the the dopant of Zr4+ can accelerate the transformation of Ti4+ to Ti3+. Moreover, when adding2 L-cystine electrocatalytic to HCl solutions, activities the reductiontoreducecurrentsL-

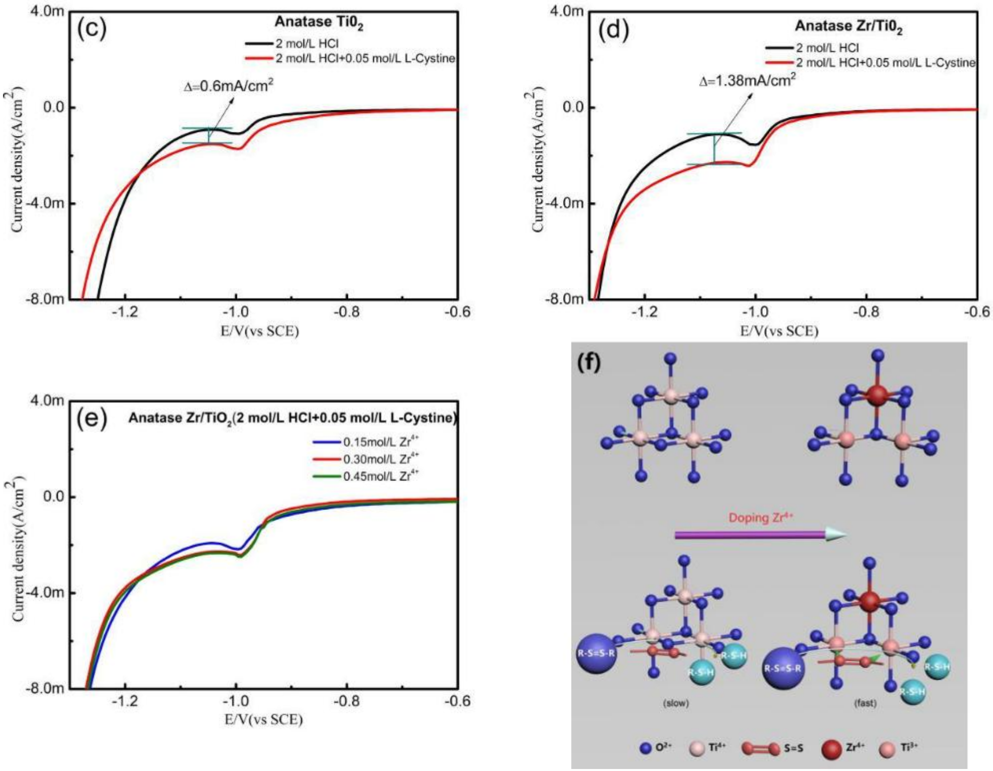

nanoarray tube, (**c**) anatase TiO2 nanoarray tube, and (**d**) anatase Zr/TiO2 nanotube array electrode; nanoarray tube, (**c**) anatase TiO$_2$ nanoarray tube, and (**d**) anatase Zr/TiO$_2$ nanotube array electrode; (**e**) the influence of concentrations of Zr(NO3)4 solution in chemical immersion process; (**f**) schematic

(**e**) the influence of concentrations of Zr(NO3)4 solution in chemical immersion process; (**f**) schematic illustration of electrocatalytic reduction mechanism of the anatase Zr/TiO2 nanotube array electrode

illustration of electrocatalytic reduction mechanism of the anatase Zr/TiO2 nanotube array electrode for L-cystine.

Conclusions

The Zr4+-doped anatase TiO2 nanotube array electrode was prepared through anodizing, The Zr^{4+}-doped anatase TiO2 nanotube array electrode was prepared through anodizing, combined with chemical immersion and heat treatment. Zr4+- doping into the anatase TiO2 induces with chemical immersion and heat treatment. Zr^{4+}-$_{doping}$ into the anatase TiO induces the transformation of Ti4+ to Ti3+ and the formation f the oxygen vacancies, improving.

Conflicts of Interest: The authors declare no conflict of interest.

References

1) Ralph, T.R.; Hitchman, M.L.; Millington, J.P.; Walsh, F.C. The reduction of l-cystine hydrochloride at stationary
2) Yang, S.; Li, G.; Liu, L.; Wang, G.; Wang, D.; Qu, L. Preparation of nickel oxide nanoparticles on N-doped *Comp.* **2017**, *691*, 834–840.
3) reduced graphene oxide: A two-dimensional hybrid for electrocatalytic sensing of L-cysteine. J. Alloy. Comp. **2017**, 691, 834–840. [CrossRef]
4) Nosal-Wiercinska,´ A. The catalytic activity of cysteine and cystine on the electroreduction of Bi(III) ions. J. Electroanal. Chem. **2011**, 662, 298–305. [CrossRef]
5) Wei, M.; Guo, J.; Shi, Z.; Yuan, Q.; Pu, M.; Rao, G.; Duan, X. Preparation and characterization of L-cystine and L-cysteine intercalated layered double hydroxides. J. Mater. Sci. **2007**, 42, 2684–2689. [CrossRef]

6) Ke, D.; Liu, H.; Peng, T.; Liu, X.; Dai, K. Preparation and photocatalytic activity of WO_3/TiO_2 nanocomposite particles. Mater. Lett. **2008**, 62, 447–450. [CrossRef]

7) Kment, S.; Riboni, F.; Pausova, S.; Wang, L.; Wang, L.Y.; Han, H.; Hubicka, Z.; Krysa, J.; Schmuki, P.; Zboril, R. Photoanodes based on TiO_2 and -Fe_2O_3 for solar water splitting-superior role of 1D nanoarchitectures and of combined heterostructures. Chem. Soc. Rev. **2017**, 46, 3716–3769. [CrossRef]

8) Qin, P.; Paulose, M.; Ibrahim Dar, M.; Moehl, T.; Arora, N.; Gao, P.; Varghese, O.K.; Grätzel, M.; Nazeeruddin, M.K. Stable and efficient perovskite solar cells based on Titania nanotube arrays. Small **2015**, 11, 5533–5539. [CrossRef]

9) Liang, X.P.; Lian, Z.W.; Zhu, J.; Men, K.; Wei, F. The preparation and properties of TiO_2 nano-porous layers for perovskite solar cells. AIP Adv. **2020**, 10, 015058. [CrossRef]

10) Ozkan, S.; Ghanem, H.; Mohajernia, S.; Hejazi, S.; Fromm, T.; Borchardt, R.; Rosiwal, S.; Schmuki, P. Boron-doped diamond as an efficient back contact to thermally grown TiO_2 photoelectrodes. ChemElectroChem **2019**, 6, 4545–4549. [CrossRef]

11) Zhang, Y.; Pan, C. TiO_2/graphene composite from thermal reaction of graphene oxide and its photocatalytic activity in visible light. J. Mater. Sci. **2011**, 46, 2622–2626. [CrossRef]

12) Zhang, W.; Shironita, S.; Umeda, M. Low Pt loading and high hydrogen oxidation reaction performance at Pt/TiO_2–SiO_2 investigated by a porous microelectrode. Catal. Lett. **2014**, 144, 112–116. [CrossRef]

13) Skúlason, E.; Bligaard, T.; Gudmundsdóttir, S.; Studt, F.; Rossmeisl, J.; Abild-Pedersen, F.; Vegge, T.; Jónsson, H.; Nørskov, J.K. A theoretical evaluation of possible transition metal electro-catalysts for N_2 reduction. Phys. Chem. Chem. Phys. **2012**, 14, 1235–1245. [CrossRef] [PubMed]

14) Hirakawa, H.; Hashimoto, M.; Shiraishi, Y.; Hirai, T. Photocatalytic conversion of nitrogen to ammonia with water on surface oxygen vacancies of titanium dioxide. J. Am. Chem. Soc. **2017**, 139, 10929–10936. [CrossRef] [PubMed]

15) Chen, X.B.; Liu, L.; Yu, P.Y.; Mao, S.S. Increasing solar absorption for photocatalysis with black hydrogenated titanium dioxide nanocrystals. Science **2011**, 331, 746–750. [CrossRef] [PubMed]

16) Song, L.; Zhang, R.; Zang, S.; He, H.; Su, Y.; Qiu, W.; Sun, X. Activity of selective catalytic reduction of NO over V_2O_5/TiO_2 catalysts preferentially exposed anatase {001} and {101} facets. Catal. Lett. **2017**, 147, 934–945. [CrossRef]

17) Krbal, M.; Sopha, H.; Pohl, D.; Benes, L.; Damm, C.; Rellinghaus, B.; Kupˇcík, J.; Bezdiˇcka, P.; Šubrt, J.; Macak, J.M. Self-organized TiO_2 nanotubes grown on Ti substrates with different crystallographic preferential orientations: Local structure of TiO2 nanotubes vs. photo-electrochemical response. Electrochim. Acta **2018**, 264, 393–399. [CrossRef]

18) Saputera, W.H.; Mul, G.; Hamdy, M.S. Ti^{3+}-containing titania: Synthesis tactics and photocatalytic performance. Catal. Today **2015**, 246, 60–66. [CrossRef]

19) Cao, N.; Chen, Z.; Zang, K.; Xu, J.; Zhong, J.; Luo, J.; Xu, X.; Zheng, G. Doping strain induced bi-Ti^{3+} pairs for efficient N_2 activation and electrocatalytic fixation. Nat. Commun. **2019**, 10, 2877. [CrossRef]

20) Shi, M.M.; Bao, D.; Wulan, B.R.; Li, Y.H.; Zhang, Y.F.; Yan, J.M.; Jiang, Q. Au sub-nanoclusters on TiO_2 toward highly efficient and selective electrocatalyst for N2 conversion to NH3 at ambient conditions. Adv. Mater. **2017**, 29, 1606550. [CrossRef]

21) Lucky, R.A.; Charpentier, P.A. N-doped ZrO_2/TiO_2 bimetallic materials synthesized in supercritical CO_2: Morphology and photocatalytic activity. Appl. Catal. B Environ. **2010**, 96, 516–523. [CrossRef]

22) Reddy, M.V.; Sharma, N.; Adams, S.; Rao, R.P.; Peterson, V.K.; Chowdari, B.V.R. Evaluation of undoped and M-doped TiO_2, where M = Sn, Fe, Ni/Nb, Zr, V, and Mn, for lithium-ion battery applications prepared by the molten-salt method. RSC Adv. **2015**, 5, 29535. [CrossRef]

23) Macak, J.M.; Gong, B.G.; Hueppe, M.; Schmuki, P. Filling of TiO_2 nanotubes by self-doping and electrodeposition. Adv. Mater. **2010**, 19, 3027–3031. [CrossRef]